Hindawi
Advances in Civil Engineering
Volume 2019, Article ID 7101982, 12 pages
https://doi.org/10.1155/2019/7101982

Research Article

Moisture Susceptibility of Warm Mix Asphalt (WMA) with an Organic Wax Additive Based on X-Ray Computed Tomography (CT) Technology

Jie Ji,[1] **Hui Yao**,[2] **Zhikai Yuan**,[1] **Zhi Suo**,[3] **Ying Xu**,[3] **Pengfei Li**,[4] **and Zhanping You**[5]

[1]*School of Civil Engineering and Transportation, Beijing University of Civil Engineering and Architecture, No. 1, Zhanlanguan Rd., Xicheng District, Beijing 100044, China*
[2]*Beijing Key Laboratory of Traffic Engineering, College of Metropolitan Transportation, Beijing University of Technology, No. 100, Pingleyuan, Chaoyang, Beijing 100124, China*
[3]*Beijing Advanced Innovation Center for Future Urban Design, Beijing University of Civil Engineering and Architecture, No. 1, Zhanlanguan Rd., Xicheng District, Beijing 100044, China*
[4]*Beijing Guodaotong Highway Design and Research Institute Co., Ltd., No. 23, Huaibaishu Rd., Xicheng District, Beijing 100053, China*
[5]*Department of Civil and Environmental Engineering, Michigan Technological University, 1400 Townsend Drive, Houghton, MI 49931, USA*

Correspondence should be addressed to Hui Yao; huiyao@mtu.edu

Received 24 October 2018; Revised 2 February 2019; Accepted 25 March 2019; Published 8 April 2019

Academic Editor: Salvatore Grasso

The warm mix asphalt was fabricated with different moisture contents (0%, 1%, 2%, and 3%) of limestone aggregates using the Superpave gyratory compactor. The moisture susceptibility of asphalt mixtures with an organic wax additive RH was studied. The samples were compacted and tested using the modified Lottman test AASHTO T283, and the X-ray computed tomography technology was used to capture the internal structure images before and after the freeze-thaw cycles. The test results show that the air voids were distributed in the size range of 0–5 mm^3 and 5–10 mm^3. The number of air voids decreased with the increase of air void size and increased after freeze-thaw cycles. The air void content can be influenced by the residual moisture in aggregates. The higher the moisture content of aggregates is, the larger the air void content is. So, the air void content is likely to be sensitive to moisture damage. The increase ratio of the air void and moisture content of aggregates had good correlation with the indirect tensile strength and tensile strength ratio of the samples. The indirect tensile strength and tensile strength ratio of the samples decreased linearly, and the samples were sensitive to the moisture damage with the increases of increase ratio of the air void/moisture content in aggregates.

1. Introduction

The technology of warm mix asphalt (WMA) features energy conservation and environmental protection, and WMA has been used widely in the industry. Different advantages are identified for WMA compared to hot mix asphalt (HMA), including (1) reduction of fuel consumption during the mixture fabrication; (2) reduction of pollutant emissions (like fumes); (3) improved compaction; (4) the possibility of longer paving seasons; and (5) lower short-term aging thanks to lower production temperatures [1–3]. Studies from the National Center for Asphalt Technology (NCAT) indicate that mixtures showed a tendency to have problems with rutting and moisture susceptibility if the mixing temperatures are reduced in WMA [4–6]. The addition of organic wax additive in mixtures affects the viscosity of asphalt binders. For WMA with organic wax additives, normally, a lower temperature is used for drying the aggregates; aggregates may not be completely dried, and some residual moisture is still in aggregates. This process may

weaken bonds and adhesions between asphalt binders and aggregates and could result in a negative impact on the moisture susceptibility of mixtures. Giuliani et al. showed that the presence of the organic wax additive in asphalt binders provided some side effects on the performance of asphalt binders, such as the reduction of the adhesions and the increased susceptibility to stripping and raveling [7]. Specifications in China and the United States require completely dry aggregates in WMA with organic wax additives [8, 9]. It is common that aggregates are stored under the cover in the field, and different heating stages are used to minimize water content in the aggregates. However, more air moisture exists due to the climate changes. Few researchers determined the influence of the residual moisture in aggregate on WMA with organic wax additives, and the residual moisture may result in moisture damage in pavements.

In most cases, the moisture susceptibility of WMA mixtures with different types of additives was studied by conventional test methods used for HMA mixtures. Hesami et al. used hydrated lime to improve the moisture susceptibility of WMA with Sasobit/Aspha-min and limestone/granite. The hydrated lime improved adhesion between asphalt binders and aggregates and reduced the probability of moisture damage in WMA mixtures [10]. The WMA mixtures with Aspha-min/Sasobit or others had a low tensile strength ratio (TSR), which is less than 0.8, and the moisture susceptibility had been improved significantly about 1.6 times with the addition of antistripping agents [11, 12]. The indirect tensile test (ITT) was used to test the WMA mixtures with freeze-thaw cycles, and TSR of WMA mixtures with the moist aggregates was lower than that of WMA mixtures with dried aggregates [13]. The residual Marshall stability and TSR of WMA mixtures declined sharply if the moisture content of aggregates increased from 0% to 2% [14]. The addition of Aspha-min/Sasobit in WMA mixtures did not have an impact on indirect tensile strength (ITS) before freeze-thaw cycles, and the resistance to deformation in WMA mixtures without moist aggregates improved [15]. The WMA mixtures with saturated surface dry (SSD) aggregates do not meet the minimum requirement of 0.80 by American Association of State Highway and Transportation Officials (AASHTO) T283 in ITT tests. The undried aggregates may have a potential of moisture damage in WMA mixtures, and the moisture susceptibility of WMA mixtures improved by incorporating hydrated lime as an antistripping agent [16]. Previous studies mentioned that the potential for moisture damage in WMA mixtures increases due to low mixing temperatures and undried aggregates. However, it is still needed to further explore how the residual moisture in aggregates affects the moisture susceptibility of WMA mixtures.

Based on the X-ray computed tomography (CT) technology, the internal structures of asphalt mixtures were analyzed [17–20]. In 1998, the Federal Highway Administration (FHWA) initiated the SIMAP (Simulation, Imaging, and Mechanics of Asphalt Pavements) program. It aimed to develop 3D image technology to capture the internal structure of asphalt mixtures and imposed loadings on the 3D numerical model to forecast the response, behavior, and performance of asphalt mixtures based on volumetric and mechanical characteristics [21–25]. The X-ray CT technology was used to determine permeability in asphalt mixtures. The air void structure was characterized, and the tortuosity of 14 samples with different total air void contents (10 of them containing limestone and 4 of them gravel) was determined. It is demonstrated that the tortuosity was in a range of 3.16 to 4.94, and the real length of a path in the samples was more than 3 times the distance between the extreme points [26]. The X-ray CT technology was adopted to analyze the internal structure of asphalt mixture and convert it into finite element software for the numerical simulation to obtain the horizontal and vertical modulus of asphalt mixture [27]. A model for the viscoplastic behavior of asphalt mixtures was developed to measure the microstructure damage with X-ray CT and image analysis techniques [28]. Duan used the X-ray CT and image processing technology to distinguish the aggregate profile and local mesostructure of asphalt mixtures and obtain a clear image of >1.18 mm aggregate through direct scanning [29]. Yong et al. established the digital image processing and X-ray CT technology to research influences of different factors on the uniformity of asphalt mixtures, such as compaction method, aggregate type, etc., [30]. Wang et al. reconstructed the asphalt mixture and analyzed the spatial distributions of aggregates, air voids, and mastic [31]. Xu et al. also described the distributions of dynamic and static moistures in the internal structure of asphalt mixtures at the microscale [32].

The Particle Flow Code (PFC) was used to study the internal structure of asphalt mixtures through X-ray scanning. The aggregate and mastic were simulated, respectively, as linearly elastic and viscoelastic bodies [33]. Wang et al. scanned the asphalt mixture and imported images into the finite element software to build the finite element model of asphalt mixtures with aggregates, air voids, and mastic. The microscopic structure model was able to reflect the internal structural characteristics of asphalt mixtures [34]. The internal structure of the asphalt mixtures was generated to study the effectiveness of two-dimensional (2D) and three-dimensional (3D) models for the simulation of the shear frequency sweep at constant height (FSCH) tests on mixtures [35]. Zelelew and Papagiannakis used volumetric thresholding algorithm, a digital image processing algorithm, to process the images of asphalt mixtures from X-ray CT scanning. The algorithm utilized volumetric properties of mixtures as the main criterion to establish the air-mastic and mastic-aggregate grayscale boundary thresholds [36]. Hamzah et al. identified the adhesion failure related to the mechanical strength and moisture damage. The area percentage of adhesion failures was quantified precisely via image analysis technique after the specimens were fractured. The analysis results show that the area of adhesion failures increased with the increase of freeze-thaw cycles. The mixtures with PG-76 binders exhibited lower failure areas compared to mixtures with PG-64 binders [37]. Alvarez focused on the analysis of the internal structure of WMA samples with three additives using both Superpave gyratory

compactor (SGC) and Texas gyratory compactor. The air void characteristics were assessed by X-ray CT and image analysis technology. The addition of WMA additives did not lead to significant changes in the vertical distribution of air voids [38, 39]. There is no significant variation in the air void characteristics of WMA samples compared to HMA samples. The use of WMA additives also did not lead to significant differences in the internal structure of the WMA mixtures compared to HMA mixtures [40]. The surface free energy (SFE) method was also used to assess the moisture damage potential of HMA, and the nanomaterials increase the wettability of asphalt binders. The aggregate surface exposed to water (P index) was introduced for the evaluation of the moisture damage in asphalt mixtures [41]. The free energy of cohesion and asphalt-aggregate adhesion have a positive effect on the moisture damage in asphalt mixtures, as well as the specific surface area of aggregates and film thickness of asphalt binders. A negative effect of debonding energy of the system and permeability of the asphalt binder was observed for the moisture damage [42].

Most of the previous studies focused on characterizing the internal structure and developing the finite element 3D numerical model for an asphalt mixture with the X-ray CT technology, but the correlation between internal structure and moisture sensitivity of asphalt mixtures, especially for WMA, is still undeveloped. The motivations of this research are to identify the moisture susceptibility of WMA with an organic wax additive based on X-ray CT technology and find the correlation between the internal structure and moisture sensitivity of WMA.

2. Objective and Scope

The objective of this research is to explain the potential for moisture damage from the mesoscale perspective using X-ray CT technology in WMA with organic wax additives. The following tasks were performed in this study in order to achieve the objective:

(i) Condition the moist aggregates with different moisture contents (1.0%, 2.0%, and 3.0%).

(ii) Design WMA mixtures with the dried/moist aggregates according to the Marshall Mix design procedures.

(iii) The modified Lottman test (AASHTO T283) is used for the WMA samples.

(iv) The X-ray CT technology is used to analyze the internal structures of the WMA samples and calculate the changes of bulk air void distribution of the WMA samples through freeze-thaw cycles.

(v) Establish the relationship between the changes of air void distribution and moisture contents in aggregates.

(vi) Analyze the correlation between the increase ratios of air voids or moisture content of aggregates and TSR and ITS of WMA.

(vii) Demonstrate the mesoscale behaviors of moisture susceptibility of WMA.

3. Experimental Program

3.1. Test Materials. An SK-90 binder with penetration grade 80/100 used in the WMA was obtained from South Korea. Limestone as a source of mineral aggregate used in the WMA was supplied by Beijing Municipal Road and Bridge Building Material Group Co., Ltd. RH as an organic wax additive is a kind of polyethylene wax and developed by Highway Science Research Institute of Ministry of Communication, which is soluble in the asphalt at the temperatures of above 100°C. RH (3% by mass of SK-90) and SK-90 were blended at 120°C and stirred 5–10 min manually. Physical properties of SK-90, RH, limestone aggregate, and chemical components are listed in Tables 1–6.

3.2. Mix Design. The asphalt mixtures with RH, an organic wax additive, were formed. The target air void of samples is $4 \pm 1.0\%$. The OAC (optimal asphalt content) of the RH-WMA (WMA with RH additive) is determined in accordance to the Marshall Mix design procedures and American Society for Testing and Materials (ASTM) D1559 (2006), and it is 4.8%. The gradation and performance of the RH-WMA are shown in Tables 7 and 8. The same parameters in the mixture design and tests were selected for all RH-WMA with dried/moist aggregates.

3.3. Conditioned Moist Aggregates. Based on the literature reviews [13, 15, 16], the oven heating method is used to condition the moist aggregates. The bucket mixer heating method was also used to condition the moist aggregates; the following procedures are seen as below:

(i) The temperature (110°C) of aggregates was determined according to the viscosity-temperature curve of the control mix binder; the viscosity-temperature curve of the control mix binder is seen in Figure 1, and its PG grades are 64-16.

(ii) The aggregates were put in the oven (110°C) more than 4 h.

(iii) The dried aggregates were poured into the bucket mixer (110°C) for keeping heat uniformity more than 30 min.

(iv) The extra distilled water (1.0%, 2.0%, and 3.0% by mass of aggregates) was added to the bucket mixer and mixed with aggregates (the 90 s) to condition the different moist aggregates.

3.4. Sample Preparation. The dried and moist aggregates with 1.0%, 2.0%, and 3.0% were conditioned in the laboratory. RH-WMA samples with dried/moist aggregates were compacted using the Superpave gyratory compactor (SGC). The mixing and compaction temperatures of control samples are 130°C and 120°C, and the mixing and compaction temperatures of RH-WMA samples (moist aggregates with 1.0%, 2.0%, and 3.0%) are 110°C and 100°C. The test samples were cylinders with 64 ± 0.5 mm in height and 100 ± 0.5 mm in diameter. A total of 4 sets of samples

Table 1: Physical properties of SK-90.

Binder	25°C penetration (0.1 mm)	15°C ductility (cm)	Softening point (°C)	60°C dynamic viscosity (Pa·s)	After RTFOT		
					Mass loss (%)	Residual penetration ratio (%)	10°C residual ductility (cm)
SK-90	80	>100	53.1	140.8	−0.113	61.6	10.1
Spec.	80–100	>100	>42	>140	≤±0.8	>50	>6

Table 2: Physical properties of RH.

Items	Density (g/cm^3)	Melting point (°C)	25°C penetration (0.1 mm)
Test value	0.914	108	0
Spec.	—	98–110	≤1

Table 3: Physical properties of coarse limestone.

Items	10–15 mm	5–10 mm	Spec.
Apparent specific gravity	2.759	2.772	>2.6
Bulk volume relative specific gravity	2.707	2.591	—
Crushing value (%)	10.1	12.1.	≤26
L.A. abrasion (%)	11.2	10.3	≤28
Soundness (%)	2.1	2.3	≤12
Soft stone content (%)	0.1	0.1	≤3

Table 4: Physical properties of fine limestone.

Items	0–5 mm	Spec.
Apparent specific gravity	2.793	>2.5
Clay content (%)	0.1	≤3
Sand equivalent (%)	73	>60
Soundness (%)	3.1	≤12

Table 5: Physical properties of fillers.

Items	Filler	Spec.
Apparent specific gravity	2.793	>2.5
Water content (%)	0.1	≤1
Hydrophilic coefficient (%)	0.03	≤1
Plasticity index (%)	1.1	≤4

Table 6: Chemical component of limestone aggregates.

Components	$CaCO_3$	SiO_2	$MgCO_3$	Fe_2O_3	CaO_2	K_2O
Content (%)	75–77	6–8	11–13	0.2–0.4	0.5–1	0.4–0.6

were fabricated. Each set contained at least 16 samples, and 64 samples totally were prepared. The bulk air void content of the samples was measured and found to be 4 ± 1.0%. The residual moisture contents of moist aggregates are 0.35%, 0.89, and 1.63%, respectively, which are corresponding to initial moisture contents of 1%, 2%, and 3%. All the RH-WMA samples were kept at room temperature for 24 h before testing.

3.5. Test Equipment. The test CT was industrial X-ray CT provided by NIKON Corporation, Japan, which essentially consisted of the following components: X-ray source, a radiation detector and collimator, image acquisition system, scanning system, data acquisition and processing system, auxiliary system, and so forth, as shown in Figure 2. The specifications and scanning parameters of the industrial CT are presented in Table 9. Industrial CT is developed based on X-ray radiographic inspection, and the operational principle is determined the specific relationship before and after X-ray beam penetrates the different materials. The X-ray absorption coefficient of a material is different; the homogeneity of scanning material is supposed. The X-ray beam attenuation equation is shown in the following equation:

$$I = I_0 e^{-\mu \Delta x}, \quad (1)$$

where I_0 is the light intensity before the X-ray beam penetrates material; I is the light intensity after the X-ray beam penetrates material; Δx is the thickness of the material; and μ is the linear attenuation coefficient of the material.

The linear attenuation coefficient of a material is not constant and varies as a function of its density. The attenuation of X-ray penetrates the materials with different penetrating energies. The tomography images of materials without overlapping are obtained by reconstruction algorithms or the distributions of linear attenuation coefficients of X-ray on cross-sections of the materials. The CT image is a map of the spatial distribution of the linear attenuation coefficient, where bright regions correspond to high values of the coefficient, vice versa. The differences in densities of two-dimensional slices were used for identification.

3.6. Test Methods

3.6.1. Moisture Susceptibility. The moisture susceptibility of the RH-WMA with dried/moist aggregates was carried out according to the modified Lottman test method (AASHTO T283). For each type of RH-WMA, two sets of unconditioned and conditioned samples were separated. The dry indirect tensile strength (dry ITS) and wet indirect tensile strength (wet ITS) were measured, and the tensile strength ratio (TSR) was also calculated.

3.6.2. Air Void. In accordance with AASHTO T269 and AASHTO T 166, the maximum theoretical specific gravity and bulk specific gravity of the RH-WMA with dried/moist aggregates were measured, and the air void percentage of the RH-WMA was calculated.

3.6.3. X-Ray CT. The industrial CT was used to scan the RH-WMA with dried/moist aggregates through freeze-thaw

Table 7: Gradation of the RH-WMA.

Sieve size (mm)	16	13.2	9.5	4.75	2.36	1.18	0.6	0.3	0.15	0.075
Lower-upper limits (%)	100	90–100	68–85	38–68	24–50	15–38	10–28	7–20	5–15	4–8
Passing ratio (%)	100	96.3	76.8	49.2	34.6	24.7	19.2	12.6	11.0	5.7

Table 8: Performances of the RH-WMA.

Items	Dynamic stability (times/mm)	Failure strain ($\mu\varepsilon$)	TSR (%)
Test results	1033.46	2194	78.39
Spec.	≥800	≥2000	≥75%

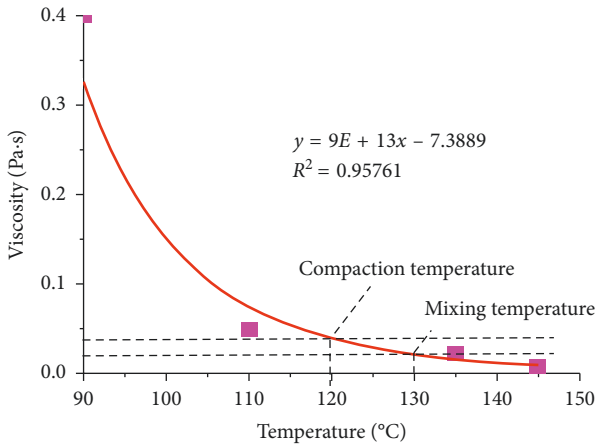

Figure 1: Viscosity-temperature curve of the control mix binder.

cycles with a 0.1 mm vertical gap, and their grayscale images were captured. The digital image processing and visual 3D reconstruction technology were used to observe and determine the change in content, size, and distribution of air voids, and the increase ratio of air voids was also calculated.

4. Results and Discussions

4.1. Image Processing Technique. An imaging processing technique is a process of converting an image into a digital form and applying various mathematical procedures to extract significant information from the image. VG Studio MAX 2.2 was used for batch processing the images of the 64 RH-WMA samples obtained from industrial CT, and the 2D images of the RH-WMA samples thereby were imported into the VG Studio MAX 2.2 software for reconstructing the 3D visual model. As the properties of aggregate, mastic, and air voids are three different phases in asphalt mixture, they can be separated, and a suitable gray intensity threshold value is determined to separate air voids from aggregate and mastic. After 3D visual model reconstruction, the air voids of the RH-WMA might be seen as a defect, and the defect analysis function of the VG Studio MAX 2.2 was selected for recognizing and analyzing air voids. Thus, the air void distribution of the samples was observed, and parameters, such as air void content, size, distribution, and connectivity, were calculated accurately.

It is complicated and important to choose a suitable gray intensity threshold in image processing. The quality of images obtained through industrial CT related to aggregate characteristics. OTSU, Gaussian mixture model (GMM), and fuzzy C-means (FCM) methods were considered and compared in order to accurately determine the gray intensity threshold value and identify air voids of RH-WMA samples [43–45]. OTUS method is an image thresholding algorithm developed by Nobuyuki Otsu. It is used to automatically perform clustering-based image thresholding or the reduction of a gray-level image to a binary image. It calculates the optimum threshold to separate two layers so that the interclass variance is maximal [43]. The procedure of OTSU is accurate and efficient, and it accommodates the actual situations by means of the iterative method. When the gray intensity threshold value was chosen for air void segmentation, repeated tests were conducted for fine-tuning to get the more accurate air void segmentation images.

The 2D and 3D air void segmentation images of the RH-WMA are shown in Figure 3. The three-phase system can be obviously distinguished from the 2D segmentation images: aggregate, mastic, and air voids. A high percentage of air voids were presented in the top and bottom regions of the RH-WMA from the 3D segmentation images. The percentage of air voids in the middle region was small and uniformly distributed. A possible explanation for this trend was the mobility of the aggregates at the top and bottom parts are restricted by the plates during the compaction procedure. Then, the coarse aggregates moved to bottom regions, and the fine aggregates were compacted densely. It is also probable that the coarse aggregates were associated with large air voids, and the top and bottom regions had less compaction than the other parts of the samples. The air void distribution related to many factors, like compaction effort, aggregate gradation, a method of compactions, etc.

4.2. Air Voids of the RH-WMA with Dried/Moist Aggregates. According to the abovementioned method for obtaining the air voids of the RH-WMA samples, VG Studio MAX 2.2 was used to calculate the air void sizes and air void contents of the RH-WMA samples with dried/moist aggregates before and after freeze-thaw cycle, respectively, as presented in Table 10. Figure 4 illustrates the relationship between the air void contents and their sizes through a freeze-thaw cycle.

From Figure 4, it can be seen that the air void contents decreased as the air void size increased before and after freeze-thaw cycles in the RH-WMA samples. It demonstrated that the air void content was 2346 pieces at the air void size of 0–5 mm^3 and dropped to 21 pieces at the air void size of 10–50 mm^3 before freeze-thaw cycles; correspondingly, the air void content was 2024 pieces at the air void size of 0–5 mm^3 and dropped to 25 pieces at the air void size of

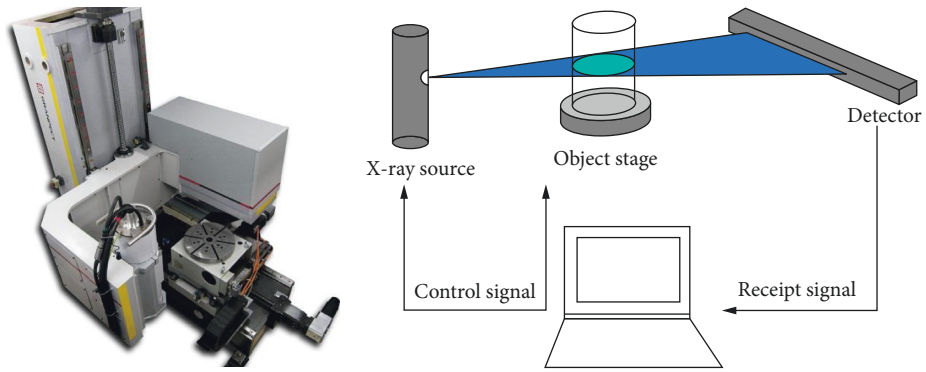

Figure 2: The schematic diagram of the industrial computed tomography (CT) system.

Table 9: Specifications and scanning parameters of the industrial CT.

Parameters	Energy	System spatial resolution	Maximum power (small/standard)	Focal size (small/standard)	Pixel size	Scan time
Spec.	600 KeV	3.0 lp/mm	700 W/1500 W	0.4 mm/1.0 mm	1024 × 1024	≤25 min

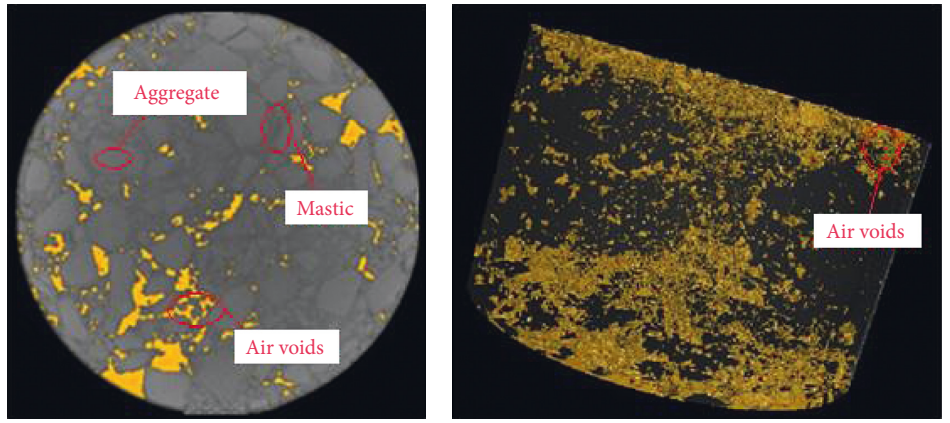

Figure 3: 2D and 3D air void segmentation images of the RH-WMA.

Table 10: Air void contents and distributions of the RH-WMA samples through freeze-thaw cycles.

Moisture content (%)	0–5 (mm^3)	5–10 (mm^3)	10–50 (mm^3)	50–100 (mm^3)	100–300 (mm^3)	300–500 (mm^3)	>500 (mm^3)	Note
0	2346	168	21	9	10	6	2	Before freeze-thaw cycle
1	2154	201	17	12	9	4	1	
2	2187	147	19	10	12	9	3	
3	2301	216	28	13	8	5	1	
0	2024	298	25	11	10	6	2	After freeze-thaw cycle
1	1854	366	32	15	11	5	2	
2	1911	280	41	14	14	10	3	
3	2004	441	46	17	12	8	3	

10–50 mm^3 after freeze-thaw cycles. Furthermore, the air void contents were mostly distributed in the air void size of 0–5 mm^3 and 5–10 mm^3, and the percentage of total air void content was more than 97%. It indicated that the air void sizes of the mixtures were small and mostly lower than 10 mm^3. The air void distributions and contents of the mixtures had similar trends with a different moisture content of aggregate.

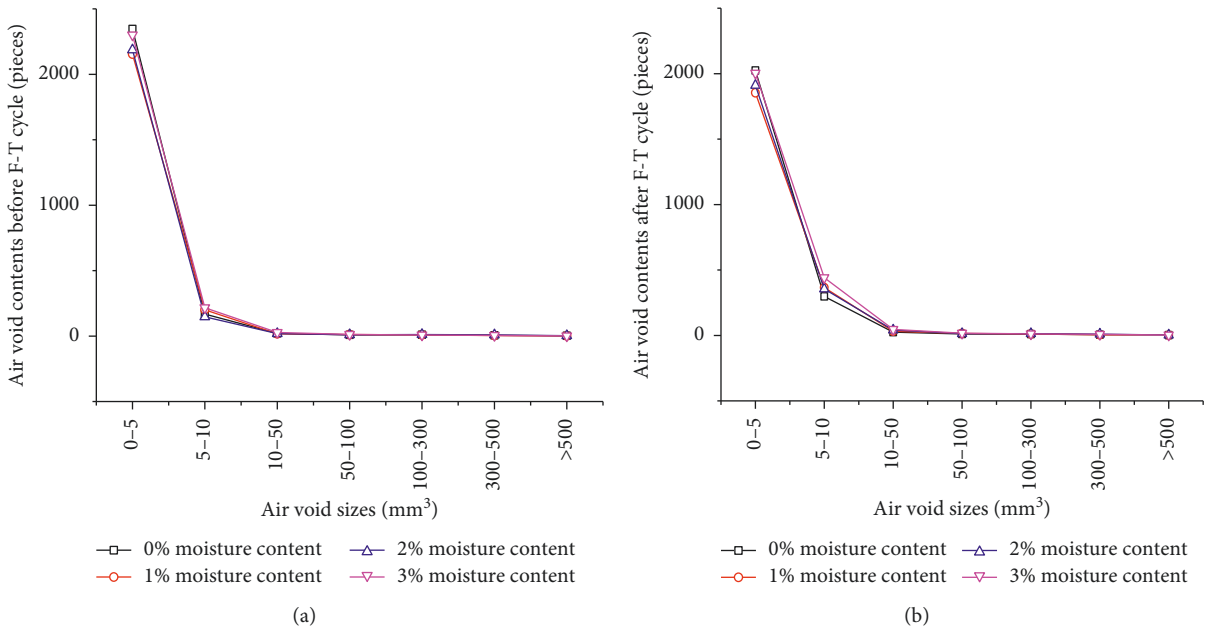

Figure 4: Air void contents and their sizes of the RH-WMA through freeze-thaw cycles.

Compared with the air void contents of the mixtures in the same air void size through freeze-thaw cycles, it is noticed that the air void content of the samples increased after freeze-thaw cycles except for the size of 0–5 mm^3 with the same moisture content of aggregates. The air void content in a range of 5–10 mm^3 after freeze-thaw cycles increased by 78%. It is worthy to note 5–10 mm^3 was an important size on the air void distribution. In general, the air void contents of the RH-WMA samples after freeze-thaw cycles increased by approximately 46.2%. This is caused by the state change of residual moisture in aggregate, such as melting and freezing, through freeze-thaw cycles.

The 5–10 mm^3 size significantly impacted the increment of the air void. The relationship between the moisture content of aggregates and 5–10 mm^3 air void contents of the RH-WMA samples was studied, and the results are exhibited in Figure 5.

Figure 5 illustrates that the moisture content of aggregate had a strong linear correlation with the increase of air void contents of the samples in 5–10 mm^3 size, and the correlation coefficient R^2 is up to 0.9510. The highest increment of air void contents was obtained for the mixtures with 3% moisture content of aggregate. In contrast, the samples with dried aggregate had the lowest increment of air void contents. This demonstrates that the mixtures with a low amount of moisture had a low increment of air voids through freeze-thaw cycles. The volume of residual moisture in aggregates was expanded up to 110% after freeze-thaw cycles. The expansion increased with the increase of residual moisture in aggregates.

According to the AASHTO T269 and AASHTO T166, the air voids of the RH-WMA samples were measured in the laboratory and denoted as MAV. The air voids of the mixtures were calculated by the images with X-ray CT technology and named as CTAV. In Table 11, the MAV and

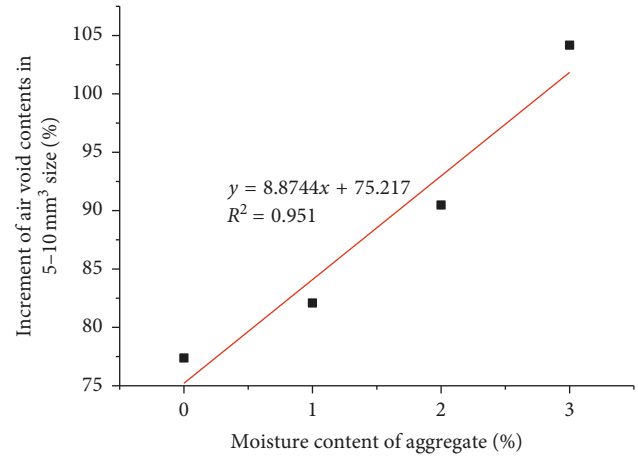

Figure 5: Moisture content in aggregates over an increment of air void contents in 5–10 mm^3 size.

CTAV values and the increase ratios before and after freeze-thaw cycles are listed, respectively.

Figure 6 presents the relationship between the moisture content and the increasing ratios of MAV and CTAV of the samples through the freeze-thaw cycles.

From Table 11 and Figure 6, the following can be found:

(i) The CTAV value was lower than the MAV value before and after freeze-thaw cycles in the RH-WMA samples with dried and moist aggregates. An explanation for this phenomenon was the difference of air void distribution between the RH-WMA samples and scanned samples. The air voids in the top and bottom regions of the samples were calculated in MAV, but not computed in CTAV. In addition, the relative error between the CTAV and MAV of the mixtures through freeze-thaw cycles was 0.0939 and

Table 11: The increase ratio of air voids of RH-WMA samples through freeze-thaw cycles.

Moisture content (%)	Before freeze-thaw cycles (%)		After freeze-thaw cycles (%)		Increase ratio of air voids (%)		Relative error (%)
	MAV	CTAV	MAV	CTAV	MAV	CTAV	
0	4.01	2.93	4.53	3.33	12.63	13.94	9.40
1	3.16	2.35	3.64	2.75	15.22	16.92	10.05
2	3.59	2.57	4.22	3.03	17.98	18.15	0.94
3	3.70	2.31	4.495	2.88	21.63	24.92	13.20
Deviation	—	—	—	—	—	—	0.0524

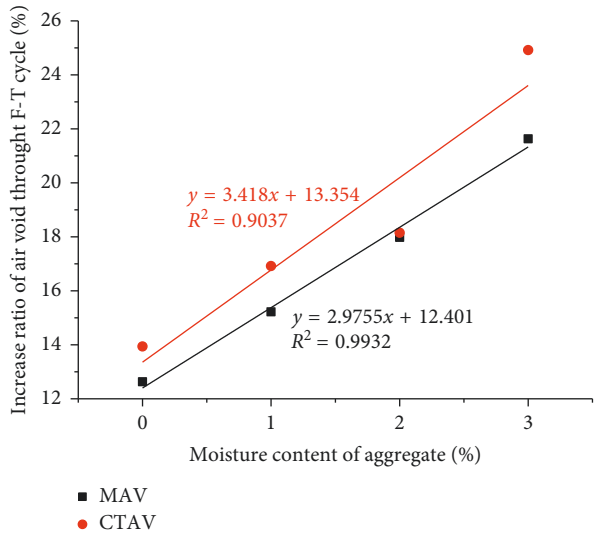

Figure 6: Moisture content in aggregates over increase ratio of air voids through freeze-thaw cycles.

0.0921, respectively. There is a good correlation between CTAV and MAV.

(ii) The CTAV and MAV of the samples with different moisture contents of aggregates before freeze-thaw cycles were lower than those after freeze-thaw cycles. The freeze-thaw cycles affected the changes of CTAV and MAV of the samples. There is a linear relationship between the increasing ratios of CTAV and MAV and moisture content in aggregate, and R^2 values are 0.9037 and 0.9932, respectively. The test results demonstrate that the increasing ratios of CTAV and MAV linearly increased as the moisture content in aggregates increased. The residual moisture in aggregates affected air void content. The higher the moisture content in aggregates is, the higher the increase ratios of CTAV and MAV are.

4.3. Air Voids of the Cut RH-WMA with Dried/Moist Aggregates. Due to a high heterogeneity in the surface region of the RH-WMA samples, the samples were cut 4 mm from the top and bottom in height and 4 mm in diameter. Thus, the samples with 56 mm in height and 96 mm in diameter were obtained, as shown in Figure 7.

Table 12 shows the CTAV of the cut samples with dried/moist aggregates before and after freeze-thaw cycles, as well as the increase ratio of CTAV. The test results indicate the freeze-thaw cycles had a significant influence on the CTAV of the cut mixtures. On the other hand, regardless of moisture contents in aggregates, the CTAV increased after the freeze-thaw cycles. The cut samples with 3% moisture content of aggregate exhibited the highest CTAV regardless of before and after freeze-thaw cycles. The moisture related to the results of CTAV. The relationships between the moisture content of aggregate and the increase ratio of CTAV through freeze-thaw cycles are shown in Figure 8.

Figure 8 demonstrates that there is a linear relationship between the moisture content in aggregates and increase the ratio of CTAV through freeze-thaw cycles for the cut samples. The correlation coefficient R^2 is up to 0.9597. The increase ratio of CTAV increased as the moisture content of aggregate increased. The higher moisture content in aggregates, the weaker the bond between the binder and aggregates is.

4.4. Image Analysis of the RH-WMA Samples with Dried/Moist Aggregates. The visual 3D model was established for changes of air voids, and the transparency was processed by VG Studio MAX 2.2. The air void distribution of the samples was determined, and it is assumed that the transparency of the 3D model was zero. The air void sizes in the same cross section of the RH-WMA samples with dried/moist aggregates before and after freeze-thaw cycles were observed. The difficult part of the process is that determination of the same cross section of the samples before and after freeze-thaw cycles. The iron wire was needed to mark and identify the same cross section position of the samples before and after freeze-thaw cycles.

The mixtures were kept in the 40°C oven for about 4 h to ensure the consistent conditions at the time of scanning and the consistent threshold value during image processing were used. The 3D images were converted into two-valued processing by Image-Pro Plus. The area with a projection of the air voids was quantified, and the changes of air voids before and after the freeze-thaw cycles were illustrated, as shown in Figure 9.

The air void sizes of the samples with dried/moist aggregates increased after freeze-thaw cycles. The air void sizes became larger compared to the analyzed images of the mixtures with dried/moist aggregates before freeze-thaw cycles. The change of air void size in RH-WMA with 3% moisture content was prominent. The more residual moistures in aggregates are, the larger the change of air void size of the RH-WMA is.

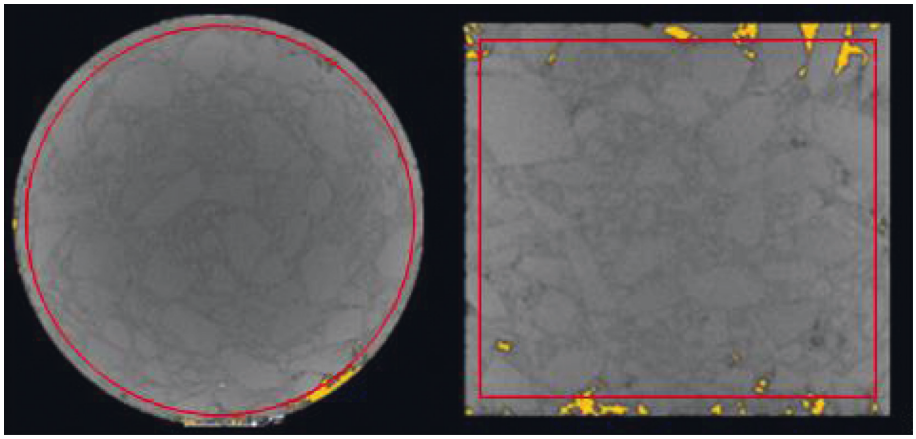

Figure 7: RH-WMA cut samples.

Table 12: The increase ratio of CTAV of the RH-WMA cut samples through freeze-thaw cycles.

Moisture content (%)	CTAV before freeze-thaw cycles (%)	CTAV after freeze-thaw cycles (%)	Increase ratio of CTAV (%)
0	1.00	1.07	5.78
1	0.97	1.05	7.71
2	1.24	1.35	8.24
3	1.31	1.43	9.56

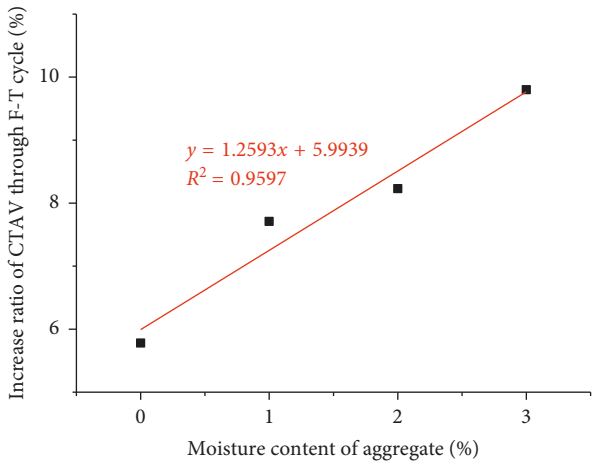

Figure 8: Moisture content in aggregates and increase ratio of CTAV through freeze-thaw cycles.

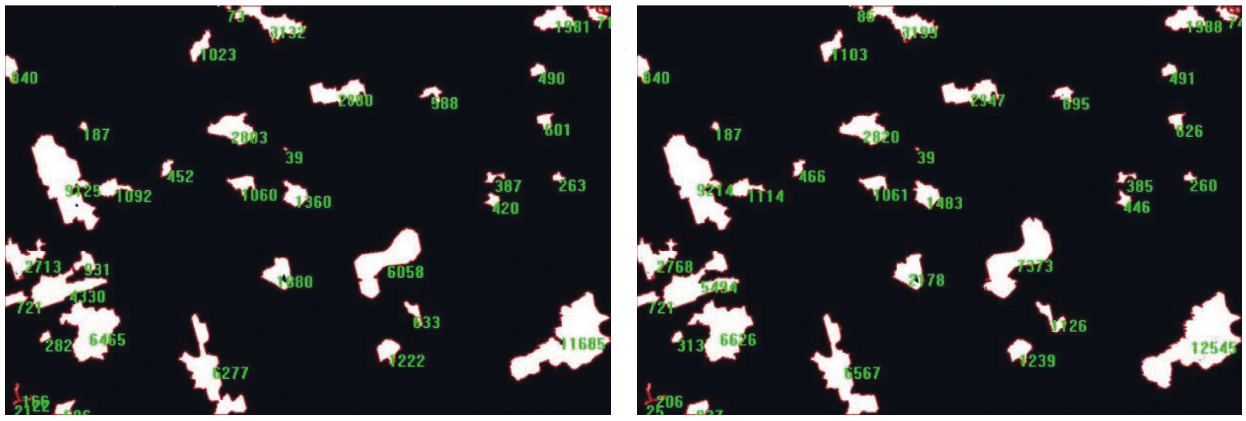

(a) (b)

Figure 9: Comparisons of air void size of the RH-WMA before and after freeze-thaw cycles. (a) The air void size before freeze-thaw cycles. (b) The air void size after freeze-thaw cycles.

4.5. Moisture Susceptibility of the RH-WMA with Dried/Moist Aggregates. The indirect tensile test was conducted on the RH-WMA with dried/moist aggregates after freeze-thaw cycles. The results for TSR of the mixtures and increase ratio of CTAV are shown in Table 13 including the dry and wet ITS of the mixtures. The test results indicate that TSR and dry and wet ITS reduced with the increase of moisture content in aggregates. Compared with 1% and 2% moisture content in aggregates, the TSR and dry and wet ITS declined more sharply in the mixtures with 3% moisture content in aggregates. It demonstrates that the mixtures with a high moisture content in aggregates can be more susceptible to moisture damage.

Figures 10 and 11 present the correlation between the moisture content of the aggregates/increase ratio of CTAV and ITS/TSR of the RH-WMA samples. A linear relation between the ITS/TSR and moisture content in aggregates through freeze-thaw cycles is shown in Figure 10. All correlation R^2 coefficients are more than 0.94. The test results exhibited that the ITS/TSR of the mixtures decreased with the increase of moisture content in aggregates. The asphalt mixtures with 3% moisture content in aggregates had the lowest ITS/TSR. Thus, it is likely that moisture susceptibility of the RH-WMA was affected by moisture in aggregates, and the moisture had a negative impact on the moisture susceptibility of the RH-WMA. The higher moisture content in aggregates is, the lower the ITS and TSR are. In other words, the RH-WMA with high moisture content is more susceptible to moisture damage.

Figure 11 illustrates that the ITS/TSR of the uncut mixtures through freeze-thaw cycles had the linear correlation with increasing ratio of CTAV; the correlation coefficient R^2 is high, and the minimum one is 0.8858. There is a good correlation between increase ratio of CTAV and ITS/TSR. The lower the ITS and TSR are, the larger the increase ratio of CTAV is. The test results present that moisture susceptibility of the RH-WMA samples was affected by a change of air voids. RH-WMA with 3% moisture content in aggregates had a large reduction in TSR and also the large increment in increase ratio of CTAV due to a large amount of moisture. Furthermore, the relative variation ratio of CTAV can be a good indicator of the moisture susceptibilities of the mixtures.

5. Conclusions

(i) The air void contents of the RH-WMA samples decreased as the air void size increased, and air void size was mostly distributed in the range of 0–5 mm^3 and 5–10 mm^3. It indicated that the morphological change of residual moisture in aggregates and freeze-thaw cycles affected on the air void distribution. During the freeze-thaw cycles, the water-ice cycles slightly expanded the volumes of air voids due to the volume changes from water to ice. From the 3D segmentation images of the RH-WMA samples, a high percentage of air voids was present in the top and bottom regions. The percentage of air voids in the middle region was small and uniformly distributed. The air void distribution related to many factors, such as aggregate gradation and method of compactions.

(ii) The higher the moisture content of aggregates is, the larger the increment of air void content is. The higher increase ratio of CTAV and MAV of the

Table 13: ITS/TSR of the RH-WMA uncut samples with dried/moist aggregates.

Moisture content (%)	Dry ITS (kN)	Wet ITS (kN)	TSR (%)	Increase ratio of CTAV (%)
0	7.11	5.00	78.39	13.94
1	6.16	4.28	73.54	16.92
2	5.61	3.64	68.99	18.15
3	5.28	3.04	61.70	24.92

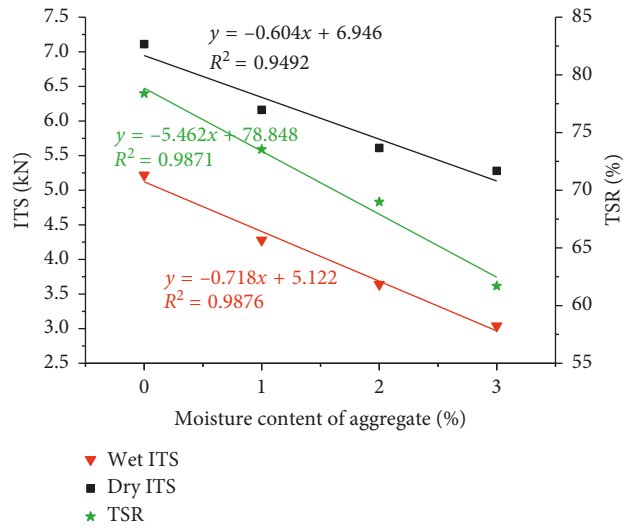

Figure 10: ITS/TSR versus moisture contents of an aggregate of the RH-WMA samples.

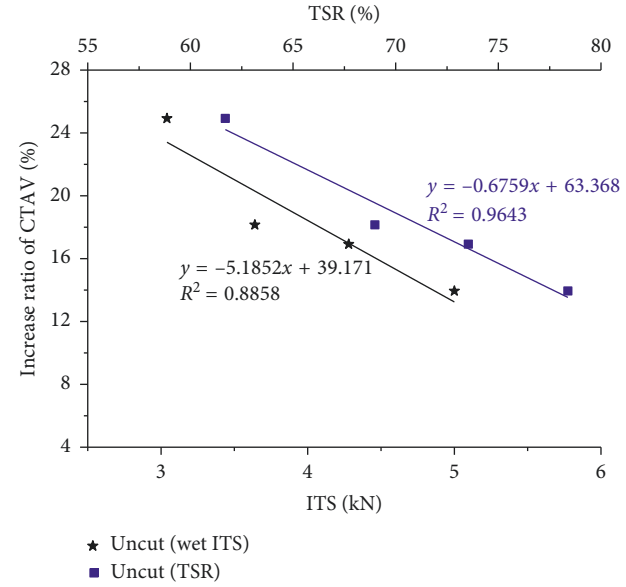

Figure 11: ITS/TSR versus increase ratios of CTAV of the RH-WMA.

RH-WMA samples was also observed. The initial moisture contents in aggregates can definitely affect the performance and volume characteristics of asphalt mixtures.

(iii) If the ITS and TSR are lower, the increase ratio of CTAV is larger. The moisture susceptibility of the RH-WMA samples was affected by changes in air voids. The ITS and TSR of the RH-WMA samples decreased with the increase of moisture contents of aggregates. There is a good linear relation between ITS/TSR of the RH-WMA samples and the moisture contents of aggregates through freeze-thaw cycles. The RH-WMA samples with the high moisture content of aggregates tend to be more sensitive to moisture damage. In addition, it is recommended that the moist aggregates are stored in the dry area and different heating steps are used for fully drying.

Data Availability

The data that support the findings of this study are available from the corresponding author upon reasonable request.

Conflicts of Interest

The authors declare no conflicts of interest.

Acknowledgments

This study was sponsored by the National Natural Science Foundation of China (51478028 and 51778038) and Program for Changjiang Scholars and Innovative Research Team in University (IRT-17R06). The authors appreciate the funding support from Beijing Key Laboratory of Traffic Engineering, Beijing University of Technology, under grant no. 2018BJUT-JTJD007. The authors also appreciate Mr. Gao Jinqi for his help in the experiments.

References

[1] R. M. Anderson, G. Baumgardner, and G. Reinke, "Engineering properties, emissions, and field performance of warm mix asphalt technologies," *Interim Report NCHRP 9-47, National Cooperative Highway Research Program (NCHRP) Transportation Research Board of the National Academies*, 2008, https://onlinepubs.trb.org/onlinepubs/archive/NotesDocs/NCHRP09-47_IR.pdf.

[2] A. J. Austerman, W. S. Mogawer, and R. Bonaquist, "Investigation of the influence of warm mix asphalt additive dose on the workability, cracking susceptibility, moisture susceptibility of asphalt mixtures containing reclaimed asphalt pavement," in *Proceedings of the 54th Annual Conference*, pp. 51–72, Washington, DC, USA, November 2009.

[3] D. Newcomb, "Warm mix: the wave of the future?," in *Proceedings of the Hot Mix Asphalt Technology*, Auburn, AL, USA, July 2005, http://www.warmmixasphalt.org/submissions/magazines/WarmMix.pdf.

[4] B. D. Prowell, G. C. Hurley, and E. Crews, "Field performance of warm-mix asphalt at national center for asphalt technology test track," *Transportation Research Record: Journal of the Transportation Research Board*, vol. 1998, no. 1, pp. 96–102, 2007.

[5] G. Hurley and B. Prowell, "Evaluation of aspha-min® for use in warm mix asphalt," NCAT Report 05-04, Auburn University, Auburn, AL, USA, 2005.

[6] G. Hurley and B. Prowell, "Evaluation of sasobit® for use in warm mix asphalt," NCAT Report 05-06, Auburn University, Auburn, AL, USA, 2005.

[7] F. Giuliani, F. Merusi, and R. Roncella, "Effects of synthetic wax on the adhesion and cohesion properties of asphalts," in *Proceedings of the International Conference on Maintenance & Rehabilitation of Pavements & Technological Control*, vol. 267, no. 18, pp. 2995–2998, Turin, Italy, July 2009.

[8] J. D' Angelo, E. Harm, J. Bartoszek et al., *Warm-Mix Asphalt: European Practice, International Technology Scanning Program Summary Report, Federal Highway Administration, U.S. Department of Transportation American Association of State Highway and Transportation Officials National Cooperative Highway Research Program*, FHWA-PL-08-007, American Trade Initiatives, Alexandria, VA, USA, 2008, https://international.fhwa.dot.gov/pubs/pl08007/pl08007.pdf.

[9] Z. F. Liu, S. P. Wu, M. Z. Chen, and D. M. Hu, "Status and problems of warm mix asphalt," *Journal of Wuhan University of Technology*, vol. 31, no. 4, pp. 170–173, 2009.

[10] S. Hesami, H. Roshani, G. H. Hamedi, and A. Azarhoosh, "Evaluate the mechanism of the effect of hydrated lime on moisture damage of warm mix asphalt," *Construction and Building Materials*, vol. 47, no. 5, pp. 935–941, 2013.

[11] S. Bhusal, "A laboratory study of Warm Mix Asphalt for moisture damage potential and performances issues," Bachelor thesis, Oklahoma State University, Stillwater, OK, USA, 2008.

[12] W. S. Mogawer, A. J. Austerman, E. Kassem, and E. Masad, "Moisture damage characteristics of warm mix asphalt mixtures," *Journal of the Association of Asphalt Paving Technologists*, vol. 80, no. 4, pp. 491–526, 2011.

[13] F. Xiao, S. N. Amirkhanian, and B. J. Putman, "Evaluation of rutting resistance in warm-mix asphalts containing moist aggregate," *Transportation Research Record: Journal of the Transportation Research Board*, vol. 2180, no. 1, pp. 75–84, 2010.

[14] W. Z. Fan, Z. X. Xie, X. S. Li, and J. N. Shen, "Study on the performance of warm mix asphalt of different aggregate water content," *Journal of Highway and Transportation Research and Development (Application Technology)*, vol. 2, pp. 100-101, 2013.

[15] F. Xiao, J. Jordan, and S. N. Amirkhanian, "Laboratory investigation of moisture damage in warm-mix asphalt containing moist aggregate," *Transportation Research Record: Journal of the Transportation Research Board*, vol. 2126, no. 1, pp. 115–124, 2009.

[16] M. R. M. Hasan, Z. P. You, D. Porter, and W. G. Shu, "Laboratory moisture susceptibility evaluation of WMA under possible field conditions," *Construction and Building Materials*, vol. 101, pp. 57–64, 2015.

[17] J. Z. Zhang, *Non-Destructive Testing Technology and Application*, Science Press, Beijing, China, 2010.

[18] R. Geng and P. Jing, "On the flourishing development of NDT techniques in China," *Journal of Mechanical Engineering*, vol. 49, no. 22, pp. 1–7, 2013.

[19] L. Tashman, E. Masad, J. D'Angelo, J. Bukowski, and T. Harman, "X-ray tomography to characterize air void distribution in Superpave gyratory compacted specimens," *International Journal of Pavement Engineering*, vol. 3, no. 1, pp. 19–28, 2002.

[20] N. Shashidhar, "X-ray tomography of asphalt concrete," *Transportation Research Record: Journal of the Transportation Research Board*, vol. 1681, no. 1, pp. 186–192, 1999.

[21] S. Taniguchi, I. Nishizaki, K. Ogawa, and J. Otani, "New X-ray CT evaluation method of engineering characteristics of asphalt mixture," in *Advances in Transportation Geotechnics 2*, pp. 400–406, CRC Press, Boca Raton, FL, USA, 2012.

[22] M. Kumagai, "A study on characteristics evaluation to control quality of asphalt mixture using X-ray CT," *Road Materials & Pavement Design*, vol. 15, no. 4, pp. 892–910, 2014.

[23] L. Wang, C. Druta, Y. Zhou, and C. Harris, "3D aggregate evaluation using laser and X-ray scanning," in *Advances in Computed Tomography for Geomaterials*, pp. 101–107, John Wiley & Sons, Hoboken, NJ, USA, 2008.

[24] L. Wang, X. Wang, L. Mohammad, and Y. Wang, "Application of mixture theory in the evaluation of mechanical properties of asphalt concrete," *Journal of Materials in Civil Engineering*, vol. 16, no. 2, pp. 167–174, 2004.

[25] Y. Fu, L. Wang, M. T. Tumay, and Q. Li, "Quantification and simulation of particle kinematics and local strains in granular materials using X-ray tomography imaging and discrete-element method," *Journal of Engineering Mechanics*, vol. 134, no. 2, pp. 143–154, 2008.

[26] A. Al-Omari and E. Masad, "Three dimensional simulation of fluid flow in X-ray CT images of porous media," *International Journal for Numerical and Analytical Methods in Geomechanics*, vol. 28, no. 13, pp. 1327–1360, 2004.

[27] L. S. Tashman, "*Internal structure analysis of asphalt mixes to improve the simulation of Superpave gyratory compaction to field conditions*," M.S. thesis, Washington State University, Pullman, WA, USA, 2001.

[28] E. Masad and N. Somadevan, "Microstructural finite element analysis of influence of localized strain distribution on asphalt mix properties," *Journal of Engineering Mechanics*, vol. 128, no. 10, pp. 1106–1115, 2002.

[29] Y. H. Duan, *Research on basic characteristics of coarse aggregates of asphalt mixture based on X-ray CT technology*, Ph.D. thesis, South China University of Technology, Guangzhou, China, 2011.

[30] P. Yong, L. J. Sun, Y. Q. Wang, and Y. J. Shi, "Application of digital image processing in evaluating homogeneity of asphalt mixture," *Journal of Jilin University (Engineering and Technology Edition)*, vol. 37, no. 2, pp. 334–337, 2007.

[31] H. Wang, Z. Huang, L. Li, X. Li, and Z. P. You, "Three-dimensional microstructural model of asphalt mixtures based on X-ray CT images," *China Sciencepaper*, vol. 8, no. 11, pp. 1115–1144, 2013.

[32] H. Xu, Y. Tan, and X. Yao, "X-ray computed tomography in hydraulics of asphalt mixtures: procedure, accuracy, and application," *Construction and Building Materials*, vol. 108, pp. 10–21, 2016.

[33] Z. You, S. Adhikari, and Q. Dai, "Air void effect on an idealised asphalt mixture using two-dimensional and three-dimensional discrete element modelling approach," *International Journal of Pavement Engineering*, vol. 11, no. 5, pp. 381–391, 2010.

[34] D. Y. Wang, W. L. Wu, X. N. Zhang, J. M. Yu, and Z. Li, "Numerical simulation of splitting test of asphalt mixture based on DIP-FEM," *Journal of Jilin University*, vol. 41, no. 4, pp. 968–973, 2011.

[35] E. Coleri, J. T. Harvey, K. Yang, and J. M. Boone, "Development of a micromechanical finite element model from computed tomography images for shear modulus simulation of asphalt mixtures," *Construction and Building Materials*, vol. 30, no. 5, pp. 783–793, 2012.

[36] H. M. Zelelew and A. T. Papagiannakis, "A volumetrics thresholding algorithm for processing asphalt concrete X-ray CT images," *International Journal of Pavement Engineering*, vol. 12, no. 6, pp. 543–551, 2011.

[37] M. O. Hamzah, M. R. Kakar, S. A. Quadri, and J. Valentin, "Quantification of moisture sensitivity of warm mix asphalt using image analysis technique," *Journal of Cleaner Production*, vol. 68, no. 3, pp. 200–208, 2014.

[38] A. E. Alvarez, J. S. Carvajal, and O. J. Reyes, "Internal structure of laboratory compacted warm-mix asphalt," *Dyna*, vol. 79, no. 172, pp. 38–45, 2012.

[39] A. E. Alvarez, N. Macias, and L. G. Fuentes, "Analysis of connected air voids in warm mix asphalt," *Dyna*, vol. 79, no. 172, pp. 29–37, 2012.

[40] J. S. Carvajal, O. Reyes, A. E. Alvarez, and L. G. Fuentes, "Evaluation of the internal structure of warm mix asphalt using X-ray computed tomography images," in *Proceedings of the International Road Federation World Meeting*, vol. 26, pp. 1–12, Riyadh, Saudi Arabia, November 2013.

[41] G. H. Hamedi and F. M. Nejad, "The employment of thermodynamic and mechanical methods to evaluate the impact of nanomaterials on moisture damage of HMA," *Materials and Structures*, vol. 49, no. 11, pp. 4483–4495, 2016.

[42] G. H. Hamedi and F. Moghadas Nejad, "Evaluating the effect of mix design and thermodynamic parameters on moisture sensitivity of hot mix asphalt," *Journal of Materials in Civil Engineering*, vol. 29, no. 2, article 04016207, 2017.

[43] S. H. Yang, "Study on the adaptive and fast algorithm of gray scale image thresholding," Master thesis, Chongqing University, Chongqing, China, 2014.

[44] A. E. Alvarez-Lugo and J. S. Carvajal-Munoz, "Practical lessons learnt from the application of X-ray computed tomography to evaluate the internal structure of asphalt mixtures," *Dyna*, vol. 81, no. 188, pp. 52–59, 2014.

[45] S. Caro, *A coupled micromechanical model of moisture-induced damage in asphalt mixtures: Formulation and applications*, Ph.D. thesis, Texas A&M University, College Station, TX, USA, 2009.